

Characterising the Internal Wave Field
of
Barkley Canyon
(Outline)

Kurtis Anstey
V00939802

Department of Physics and Astronomy
University of Victoria
August 13, 2021

Dr. Jody Klymak (University of Victoria)
Dr. Steven Mihaly (Ocean Networks Canada)
Dr. Richard Thomson (Institute of Ocean Sciences)

Table of Contents

List of Figures	3
1 Abstract	4
2 Introduction	4
3 Theory	5
4 Data	6
5 Methods	9
6 Results	10
6.1 Inter-annual regularity	10
6.2 Observed currents	10
6.3 Frequency response	14
6.4 Topographic effects	15
6.5 Seasonality	16
6.6 Continuum response	17
7 Summary and discussion	18
8 Conclusions	19
9 Appendix A: Inter-annual comparisons	20
10 Appendix B: Frequency band comparisons	22
11 References	26

List of Figures

1	Internal wave processes	4
2	Internal waves and topography	5
3	Internal waves in a two-layer system	5
4	Radiating internal waves in a lab	6
5	Barkley Canyon site and M2 criticality	7
6	Site topography	8
7	Averaged stratification and WKB scaling	9
8	Velocities - Low-pass - 2013	11
9	Velocities - High-pass - 2013	13
10	Power spectra - 2013	14
11	Rotary spectra - 2013	15
12	Continuum GM comparison	18
13	Depth-band PSD - Upper Slope - 2013	22
14	Depth-band rotary spectra - Upper Slope - 2013	23
15	Depth-band PSD - Axis - 2013	24
16	Depth-band rotary spectra - Axis - 2013	25

1 Abstract

Concise summary of each section in thesis ($\sim 1/2$ page).

2 Introduction

Internal waves general description and importance (Figure 1).

Internal waves history of research (Figure 1).

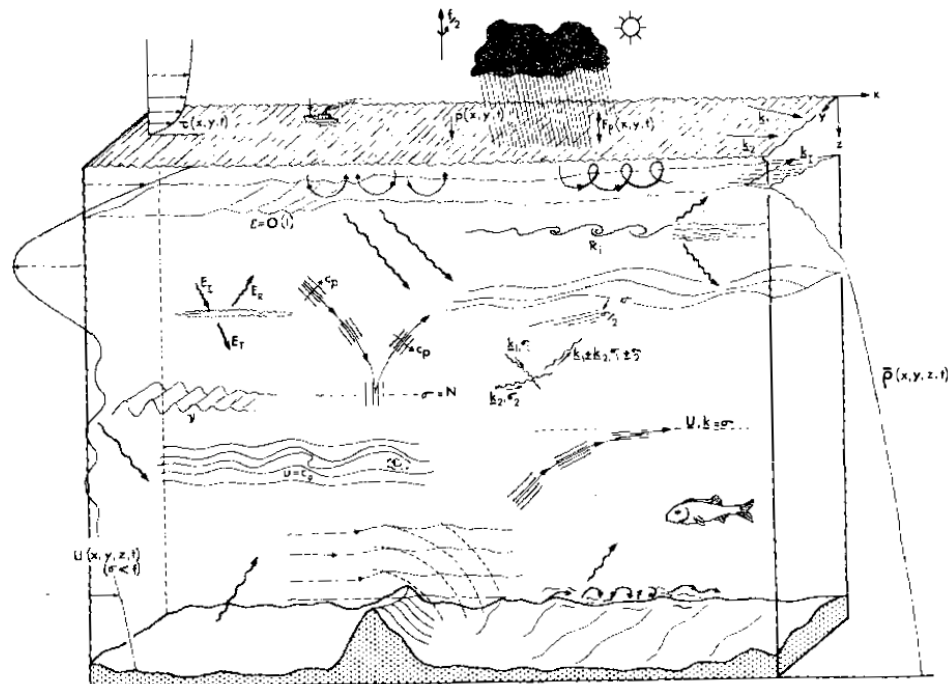


Figure 1: Generalised depiction of internal wave processes in the ocean, as envisioned by Garrett and Munk (1979). Internal waves are forced by, coincide with, or contribute to most physical processes in the ocean.

Internal waves at topography (Figure 2).

Internal waves at topography notable studies (Figure 2).

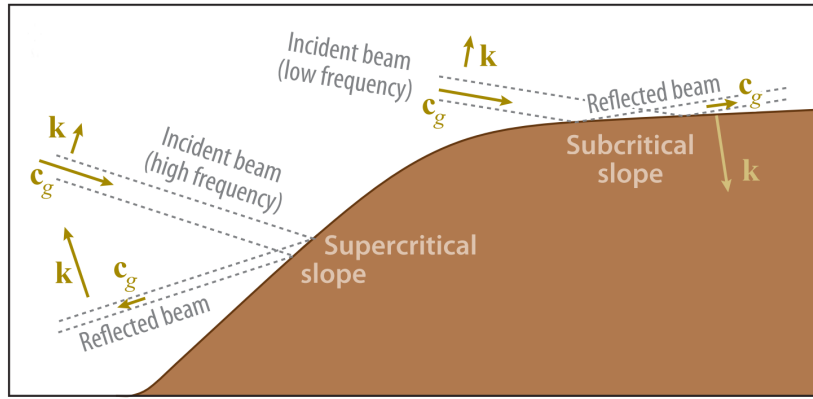


Figure 2: Graphic of internal wave interactions with slope topography (Lamb, 2014). Internal wave propagation angle depends on frequency, and depending on the slope of the encountered topography can be scattered up, reflected down, or focused.

Local / Canadian research and importance.

Gaps in research and how this study will contribute.

3 Theory

Dependence on stratification (Figure 3).

Buoyancy effects.

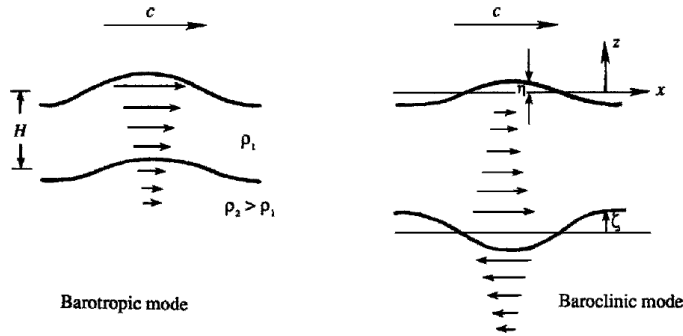


Figure 3: Internal waves in a two-layer system. Graphic representation of the difference between barotropic and baroclinic flow. Adapted from Kundu & Cohen (2008).

Additional assumptions and governing equations.

Dispersion relation.

Restricted between f and N .

Group velocity and phase speed (Figure 4).

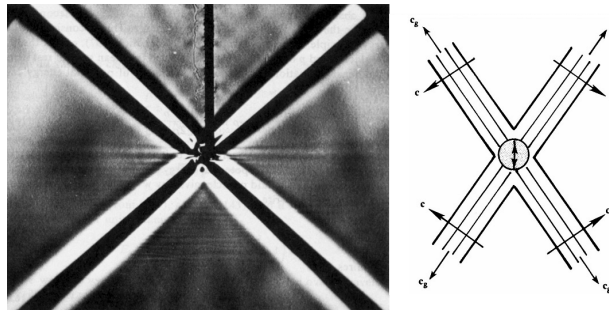


Figure 4: A photograph and graphic showing laboratory evidence for the radiation of 2D internal waves, from a source. Note the perpendicular phase and group velocities, and distinct propagation angles. Adapted from Kundu & Cohen (2008).

Angle of propagation (Figure 4).

Criticality of topography (reflection, scattering, focusing).

4 Data

Uniqueness of dataset.

Site description and ONC (Figure 5).

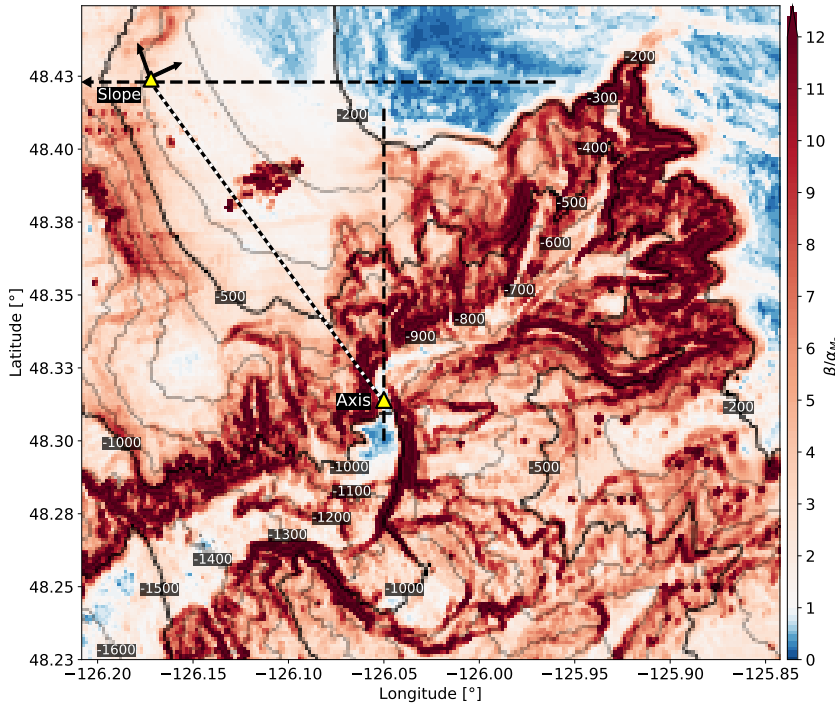


Figure 5: Site map and semidiurnal criticality of Barkley Canyon. Criticality is found by dividing the gradient slope of topography by the semidiurnal propagation angle. Most of the region is supercritical ($\zeta > 1$) to the M_2 internal tides, with notable exceptions on the shelf and canyon floor near the Axis site. Arrows at the Slope site indicate rotation of velocity data to match approximate along-slope (v) direction of mean currents; Axis data were not rotated, and the along-canyon (v) component is aligned N-S. Dashed black lines indicate topography cross-sections used in Figure 6, and the dotted black and white line represents the 15 km horizontal distance between sites. ADJUST QUALITY FOR FINAL DRAFT.

Instrument parameters (Figure 6).

Data coverage and quality checks (Figure 6).

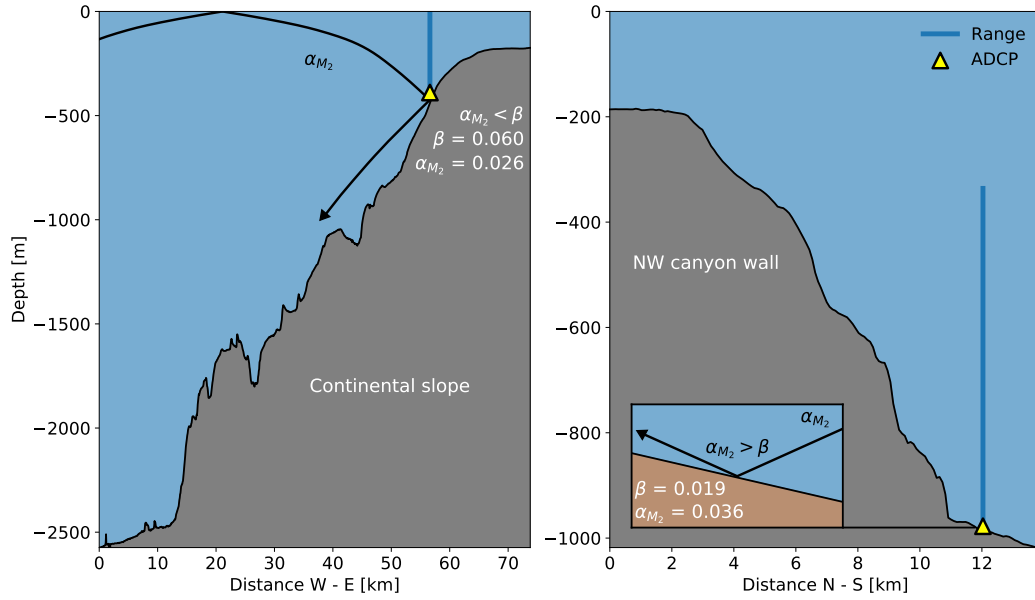


Figure 6: Site topography cross-sections with ray tracing. Depicted are the relative locations for Slope (left) and Axis (right) instrument moorings. Horizontal cross-sections were taken in the W-E (Slope) and N-S (Axis) directions, represented by the dashed black lines in Figure 5. Slope sits below the VICS shelf-break while Axis is located on the floor of Barkley Canyon (right). An incident ray is shown for M_2 , accounting for depth-dependent stratification, as well as local criticality at each site. α is the angle of propagation, and β is the slope of the topography. In general, the Slope region is supercritical while the Axis region is both subcritical (floor) and supercritical (walls).

Data management and preliminary processing.

Supplemental data and processing (climatology and buoyancy (Figure 7), bathymetry (Figure 5), wind (Figure ??), surface-level (Figure ??)). *Figures for wind and surface-level to be added to section on forcing for near-inertial and tidal bands.*

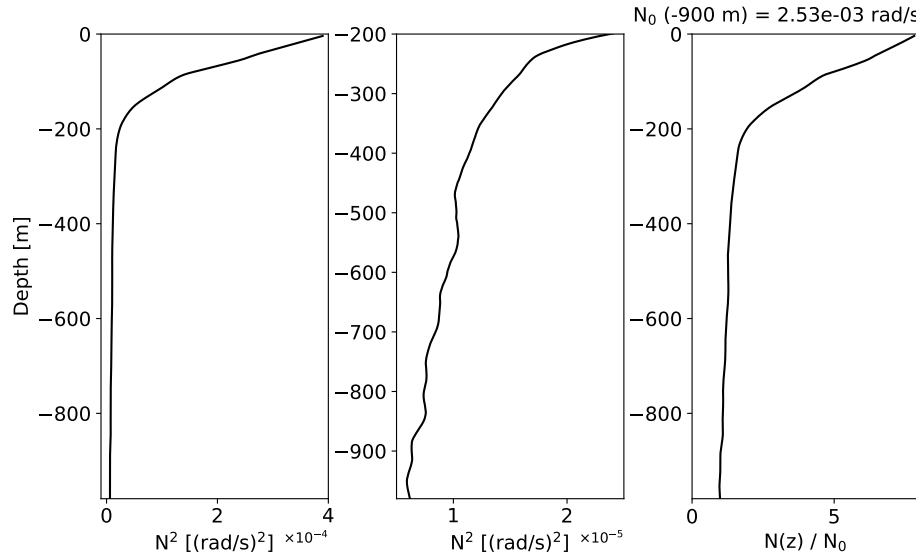


Figure 7: N^2 parameter and WKB scaling factor. Buoyancy results were averaged and smoothed from 10 years of La Perouse station LB14 CTD data, and are displayed through the water column (left) and below -200 m (centre). Depth-dependent buoyancy versus reference buoyancy (right) was determined for use in Equation ??, based on N_0 averaged around -900 m.

5 Methods

Some of this can likely be moved to appropriate results sections.

Rotation of Slope data (Figure 5).

WKB scaling (Figure 7).

Noise floor estimates for spectra (Figure 10).

GM spectrum (Figure 10).

Rotary spectral analysis and GM consistency relation (Figure 11).

Near-inertial slab model (Figure ??). *Figure for slab model output will be added to near-inertial forcing section.*

Near-inertial pumping extension (Figure ??). *Figure for pumping extension output will be added to near-inertial forcing section.*

Near-inertial vertical mode decomposition (Figure ??). *Figure for vertical*

mode output will be added to near-inertial forcing section.

Dissipation rates (Figure ??) and diffusivity (Figure ??). *Figures for dissipation and diffusivity will be added to continuum analysis section.*

6 Results

6.1 Inter-annual regularity

Describe a few examples of inter-annual regularity in seasonality that exists in the data, to justify using 2013 as a reference year.

Refer to Appendix A: Inter-annual comparisons for complete set of comparison plots. *Is this necessary, or too much? That's four per site (each year), per analysis, which adds up (and sometimes each of those has two components, or five bands!). Could refer reader to GitHub archive instead?*

6.2 Observed currents

A short section introducing the observations.

Summary:

Mean currents are as expected for this region. Topography guides flow.

Observations:

Mean currents (40h low-pass) (Figure 8):

Seasonal switch from poleward to equatorward upwelling favourable currents at Slope.

Topographically guided. Mostly along-slope and along-canyon.

Slightly stronger near topography at Slope. Generally weaker with subtle depth dependence and seasonality in the canyon.

Comparison and speculation: California Undercurrent, etc.

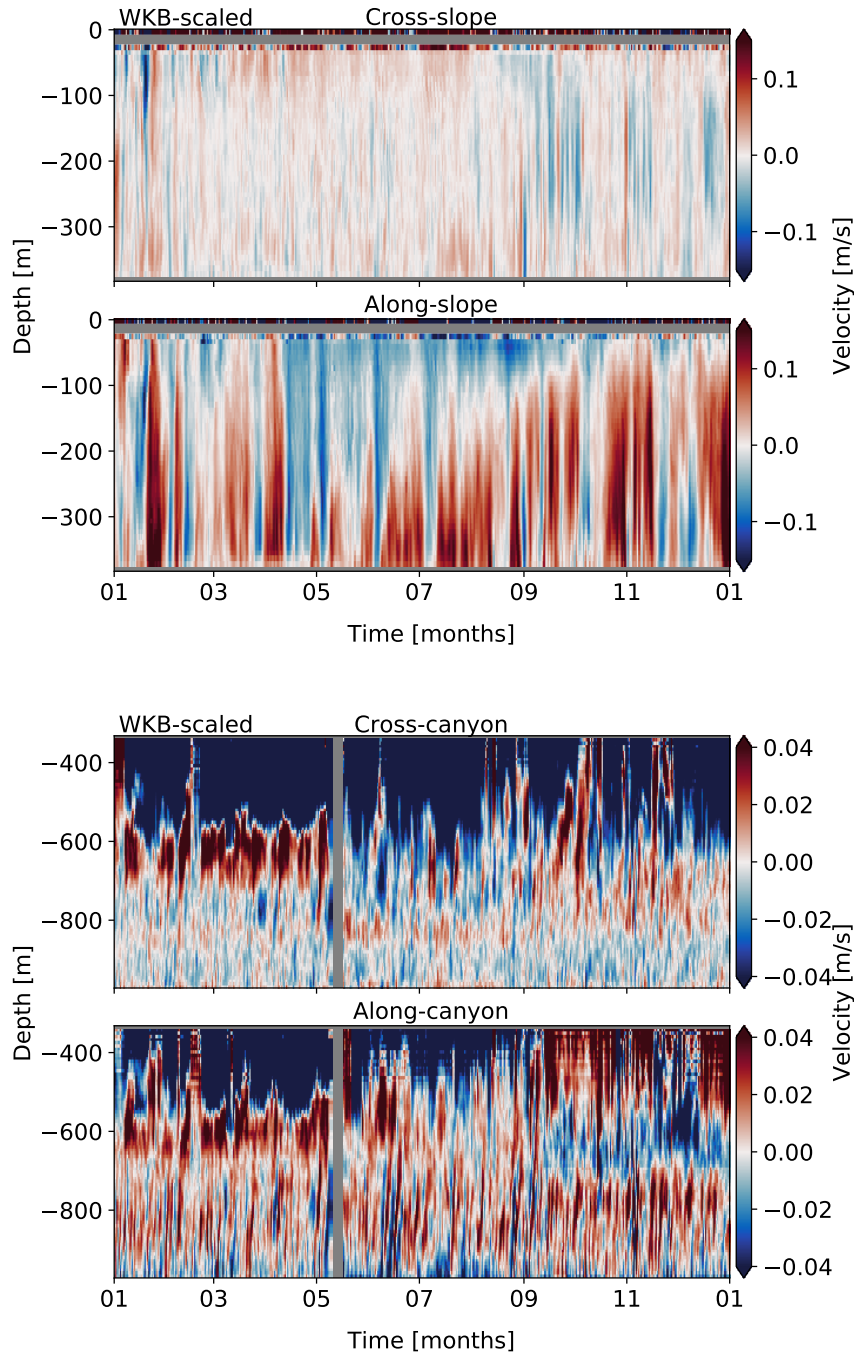


Figure 8: 40-hour low-pass horizontal velocity data for Slope (top) and Axis (bottom), in 2013. For each, components are separated as cross- (upper) and along-slope/canyon (lower). Velocities are 'adjusted', in that they have been rotated, NaN-interpolated, and WKB-scaled as detailed in section 4. There is a clear seasonal cycle in the along-slope component at Slope, while seasonality is less apparent either component at Axis.

Tidal currents and internal waves (40hr high-pass) (Figure 9):

Presence of internal waves and tides of different frequencies, directions, and vertical structure.

Strongest near to topography, at both sites.

Comparison and speculation: Internal tides generated at topography. Near-inertial internal waves generated at surface.

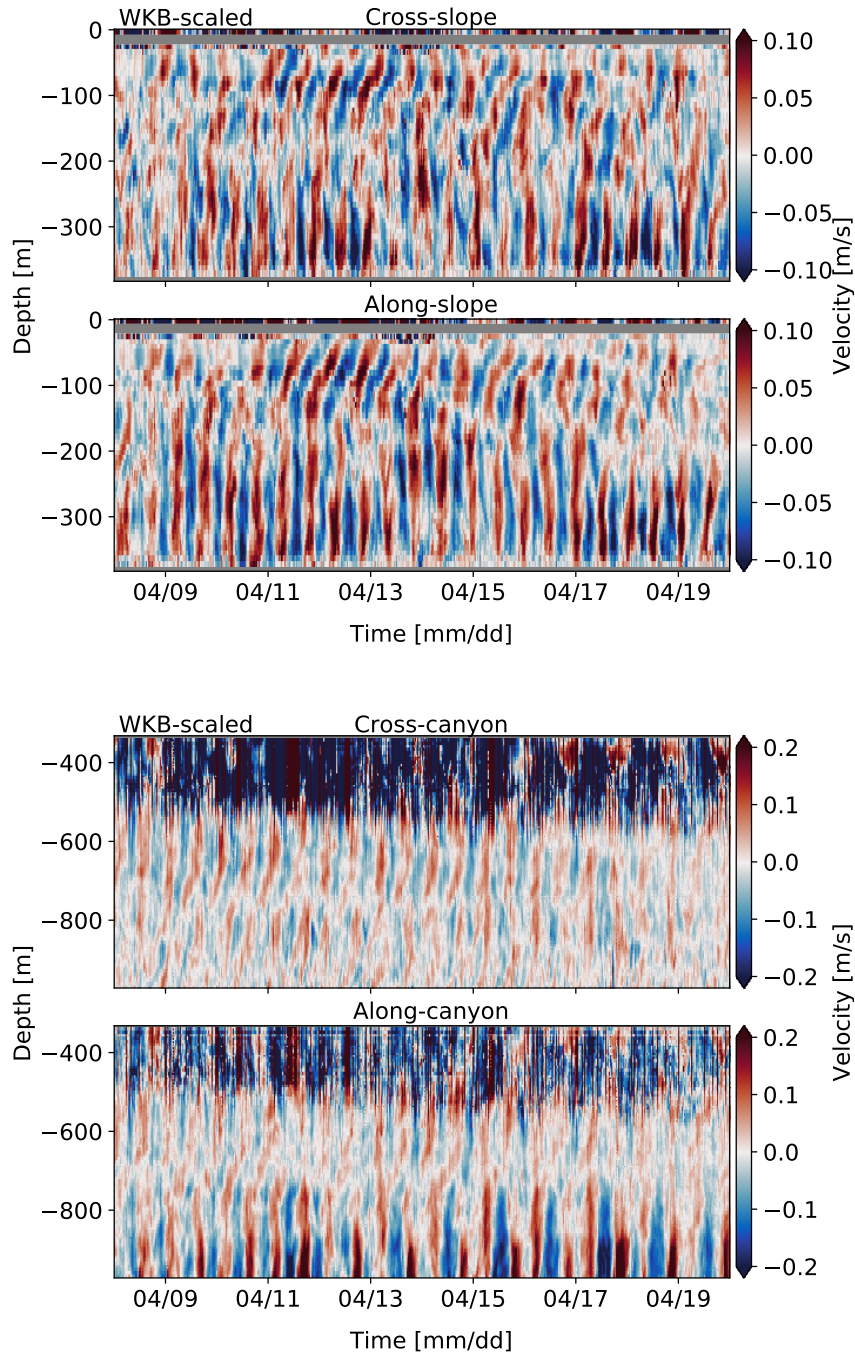


Figure 9: 40-hour high-pass horizontal velocity data for Slope (top) and Axis (bottom), in April 2013. For each, components are separated as cross- (upper) and along-slope/canyon (lower). Velocities are 'adjusted', in that they have been rotated, NaN-interpolated, and WKB-scaled as detailed in section 4. There are clear internal waves and tides of varying frequency and vertical structure, as well as depth-dependent intensity most notably along-canyon near the bottom.

6.3 Frequency response

Summary:

K1, f, and M2 dominate. Sub-K1 strong at Slope, and high-frequency continuum appears heightened and whitened versus GM.

Observations:

Diurnal, inertial, and semidiurnal dominate, with certain sum frequencies present.

Depth-specific spectra at Slope show diurnal = inertial < semidiurnal.

Depth-specific spectra at Axis show inertial < diurnal < semidiurnal.

Subdiurnal motions are stronger at Slope than Axis.

Continuum appears heightened at Axis compared to Slope.

Comparison and speculation: Depth and/or topography likely effects strength of constituents.

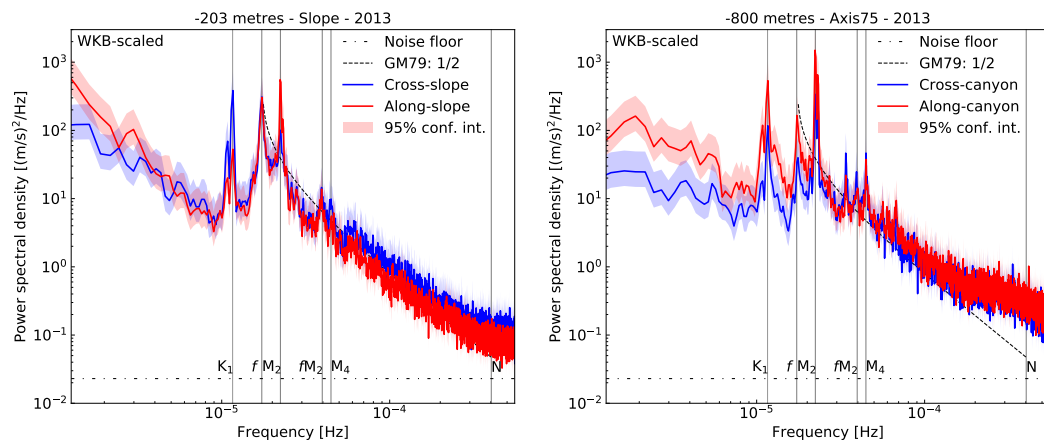


Figure 10: Time-mean PSD for Slope (left) and Axis (right) in 2013, from horizontal velocity data. Both cross- (blue) and along-slope/canyon (red) components are shown with 95% confidence intervals (shaded). For reference, the instrument noise floor (dotted line), component-wise GM79 spectrum (dashed line), and key frequency constituents (vertical lines) have been included. Spectra at both sites are characteristically red, with sharp tidal and near-inertial peaks. *Plot band ranges. Remove titles, but not depths.*

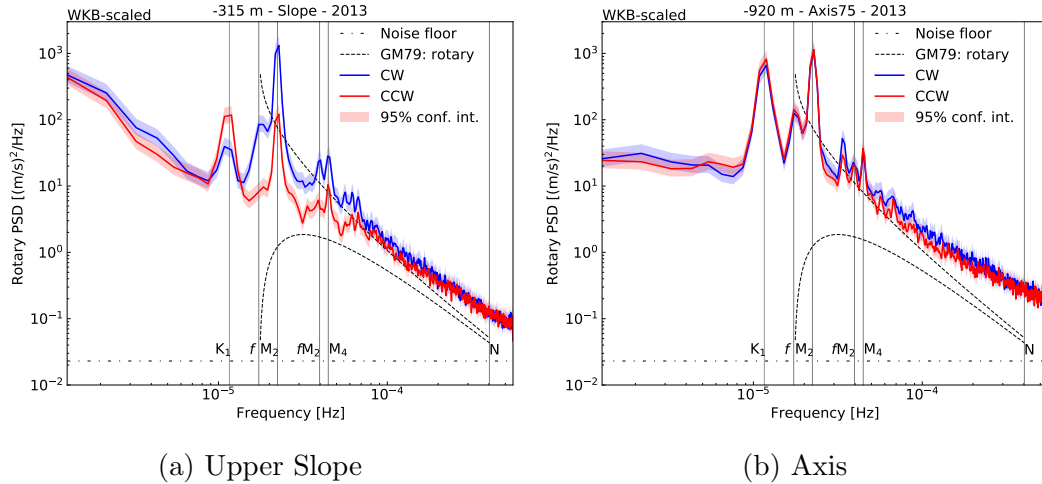


Figure 11: Time-mean rotary spectra for (a) Upper Slope and (b) Axis in 2013, from adjusted horizontal velocity data. Both CW (blue) and CCW (red) components are shown for comparison, with 95% confidence intervals. For reference, the instrument noise floor (dotted line), rotary GM79 spectrum (dashed lines), and key frequency constituents (vertical lines) are shown.

6.4 Topographic effects

Summary:

Enhancement near topography (2x orders of magnitude 150 m AB at Slope, 3x orders of magnitude 250 m AB at Axis). Subdiurnal and diurnal primarily along-slope (trapped to topography). Most of the region supercritical to semidiurnal (downward), except canyon bottom (upward). **Near-inertial attenuated at slope, enhanced in canyon.** Continuum less directional.

Slope effects (depth-frequency plots):

Subdiurnal mostly along-slope, enhanced 150 m AB.

Diurnal mostly along-slope, enhanced 150 m AB.

Near-inertial downward, attenuates 150 m AB.

Semidiurnal downward, enhanced 150 m AB.

Continuum mix of components, enhanced 150 m AB.

Comparison and speculation: Sub-inertial trapped subdiurnal and diurnal signals. Downward near-inertial absorption by increased vertical shear in background flow near topography. Semidiurnal free and supercritical for most of

slope region, leads to dominantly downward reflection. Continuum due to dissipative effects near topography, will be discussed further, later.

Canyon effects (depth-frequency plots:)

Subdiurnal mostly along-canyon, enhanced 250 m AB.

Diurnal mostly along-canyon, enhanced 250 m AB.

Near-inertial along-canyon, enhanced 250 m AB.

Semidiurnal along-canyon (some cross-canyon), enhanced 300 m AB (100 m AB).

Continuum mix of components, enhanced 300 m AB.

Comparison and speculation: Sub-inertial trapped subdiurnal and diurnal signals, as at Slope. Near-inertial canyon flow forced externally, radiates at depth due to interactions with canyon floor and walls. Semidiurnal free, but supercritical walls lead to downward reflection while subcritical floor leads to upward reflection, causing waves to be 'trapped' at depth. Continuum due to dissipative effects near topography, will be discussed further, later.

6.5 Seasonality

Summary:

Enhancement seasonality varies between bands, but little inter-annually. Similar for diurnal and semidiurnal, but barotropic forcing is local for diurnal and remote for semidiurnal. **Near-inertial forcing speculation through slab model, pumping, and vertical modes.**

Subdiurnal and tidal seasonality (integrated depth-band power):

Subdiurnal subtle seasonality, lull in summer. Similar at both sites.

Diurnal strong pulse in late-spring. Similar at both sites. In phase with barotropic surface levels, local forcing.

Semidiurnal similar to diurnal at Slope, but less obvious in canyon. Out of phase with barotropic surface levels, remote forcing.

Comparison and speculation: Sub-inertial seasonality is unclear, will research. Diurnal likely tied to changes in stratification and regional mean currents. Semidiurnal similar to diurnal, but muddled in the canyon due to topographic effects (bouncing off walls/bottom).

Near-inertial seasonality:

Near-inertial intermittent pulses, strongest in winter and fall.

More at Slope, mostly only fall pulses showing up in canyon.

Pulses align with near-inertial forcing by certain regional wind events.

Comparison and speculation: Near-inertial associated with particular wind events contributing to near-inertial energy pumping the mixed layer, with only the most significant events getting into the canyon.

6.6 Continuum response

Summary:

State of continuum reflects topographic effects. Continuum elevated compared to GM (slope and amplitudes) near topography at both sites. Dissipation and diffusivities reflect this. **Continuum seasonality suggests a cascade of energy from trapped subinertial motions at Slope, and canyon trapped semidiurnal motions in the canyon.**

Continuum enhancement and seasonality:

c/GM amplitudes are generally heightened to many times the expected GM energy. Near to the slope, and everywhere in the canyon (though most of all near the bottom).

Dissipation estimate exceed 10^{-8} W/kg near topography.

Diffusivities exceed 10^{-3} m²/s near topography.

Similar seasonality to the subdiurnal (and somewhat the diurnal) band at Slope, and the semidiurnal (and maybe a few near-inertial events) at Axis. Slopes are whitened compared to the GM expected -2 for the open-ocean, increasingly so near topography.

Comparison and speculation: At Slope, the trapped subdiurnal (strong) and diurnal waves can only propagate along topography, causing significant dissipation through a cascade of energy from low to high frequency motions. Similarly, at Axis, the strong 'canyon trapped' semidiurnal signal shows significant topographic interaction, and hence high rates of dissipation contributing to high-frequency motions.

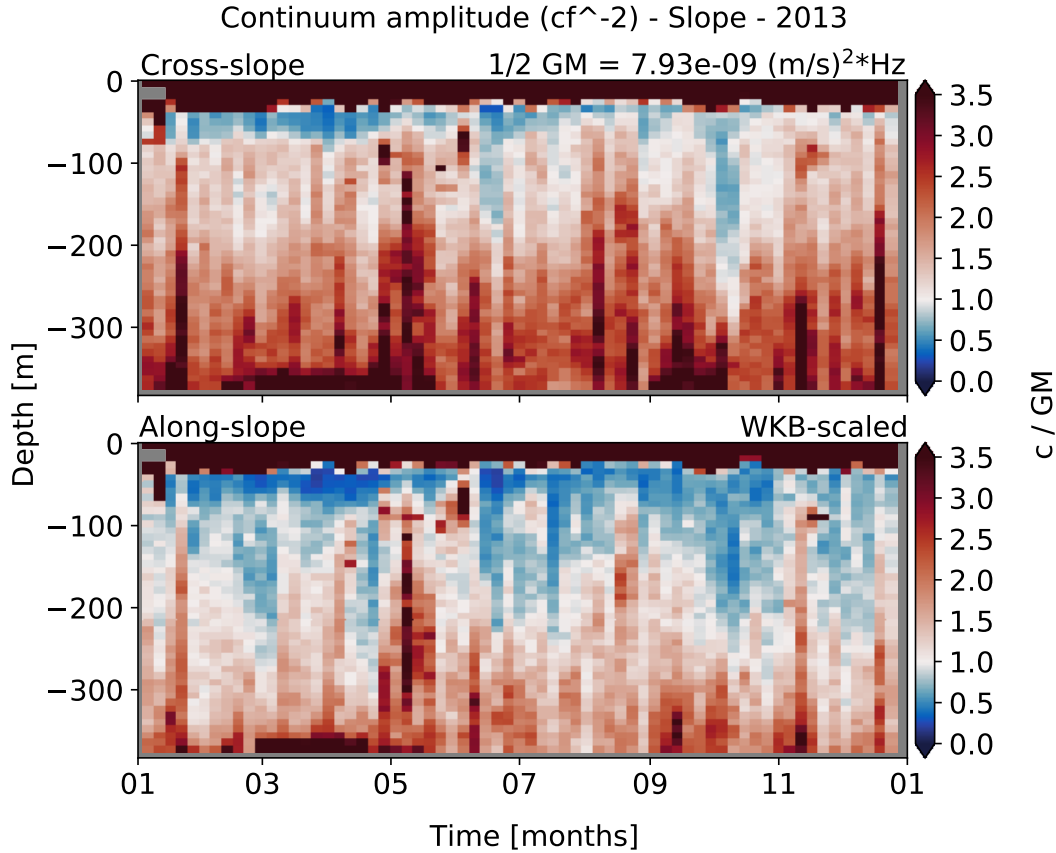


Figure 12: Continuum amplitude (c) versus GM amplitude over the same frequency bandwidth, for Upper Slope in 2013. Results are obtained from WKB scaled spectra. Continuum component amplitudes are divided by the $1/2$ GM amplitudes determined using the same method to show elevated (red) and reduced (blue) high-frequency internal wave energy through depth and time. Internal wave energy is generally enhanced near topography, as compared to the open-ocean.

7 Summary and discussion

Summary.

Expanded possible explanations and connections (where necessary).

Additional speculation.

(Supplemental figure.)

Sources of error and improvements.

Potential for future research.

8 Conclusions

Recap of each section, highlighting main points.

Key take-away from research (reiterate importance).

9 Appendix A: Inter-annual comparisons

Is this necessary, or too much? That's four per site (each year), per analysis, which adds up (and sometimes each of those has two components, or five bands!). Could refer reader to GitHub archive instead?

10 Appendix B: Frequency band comparisons

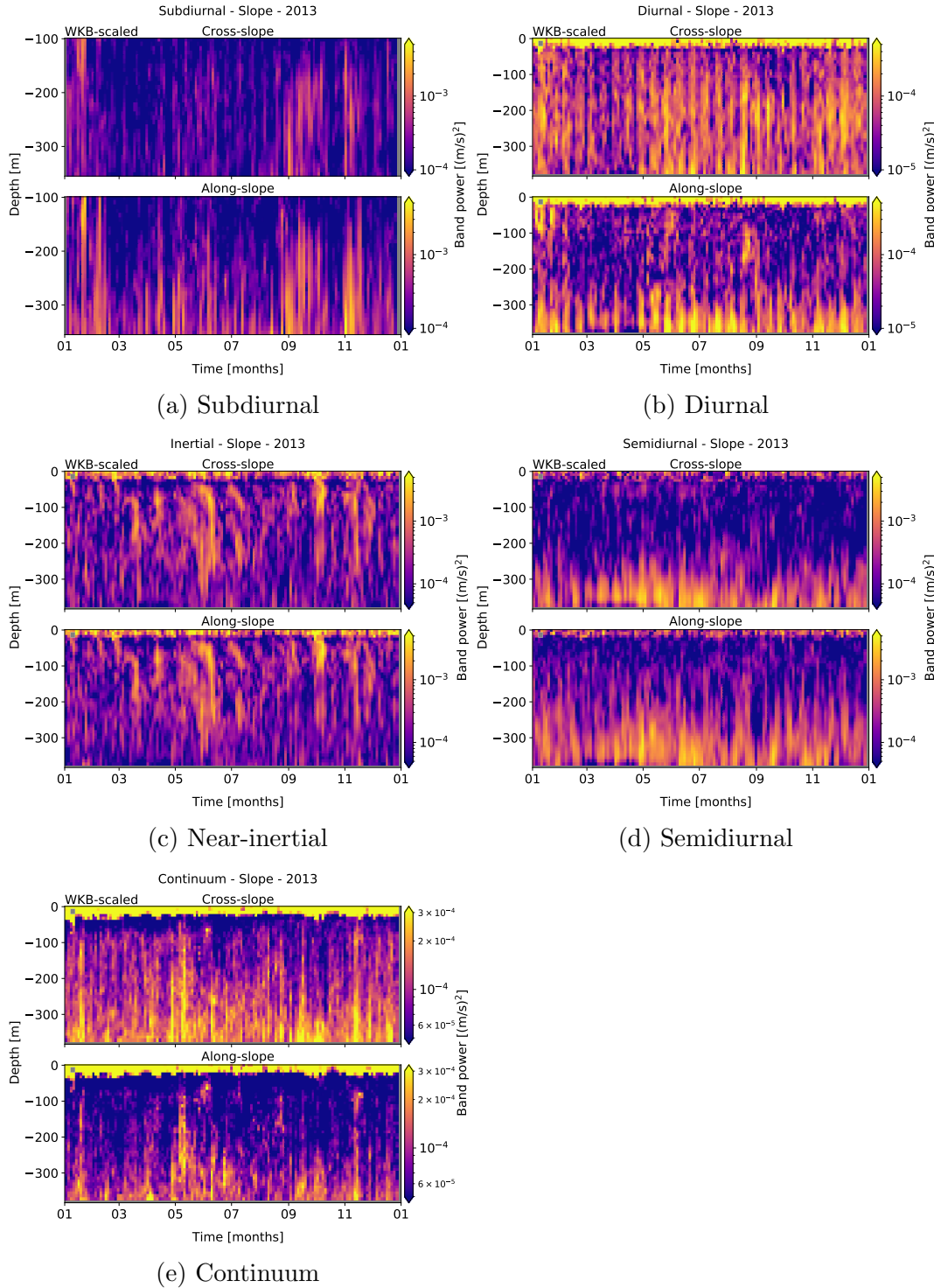


Figure 13: Band-intergrated PSD data for Upper Slope in 2013, for rotated, cleaned, and WKB-scaled horizontal velocity data. For each sub-figure, there are cross- (top) and along-slope (bottom) components. Intensity scales are adjusted for visual clarity of effects.

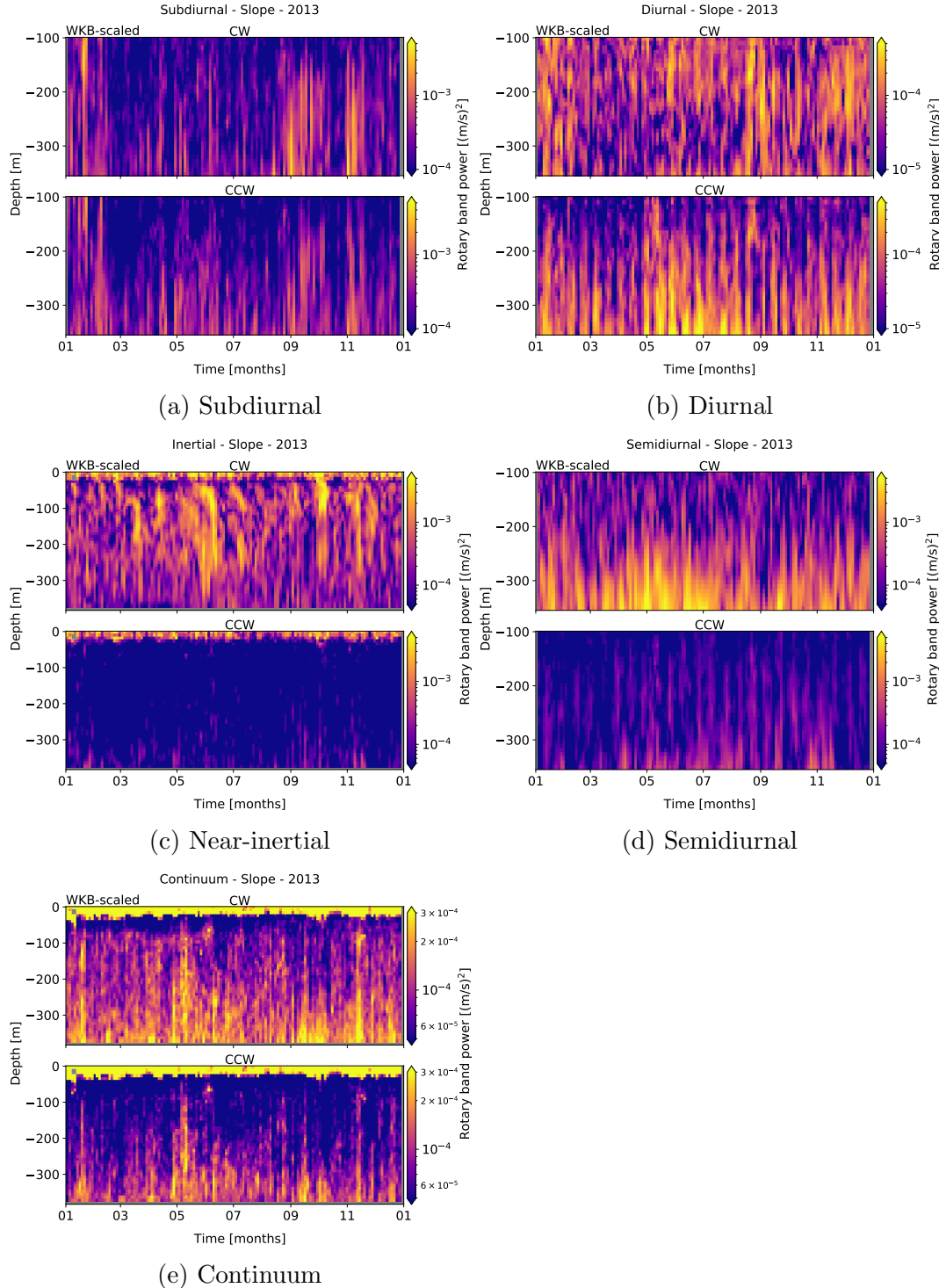


Figure 14: Band-integrated rotary data for Upper Slope in 2013, for rotated, cleaned, and WKB-scaled horizontal velocity data. For each sub-figure, there are CW (top) and CCW (bottom) components. Intensity scales are adjusted for visual clarity of effects.

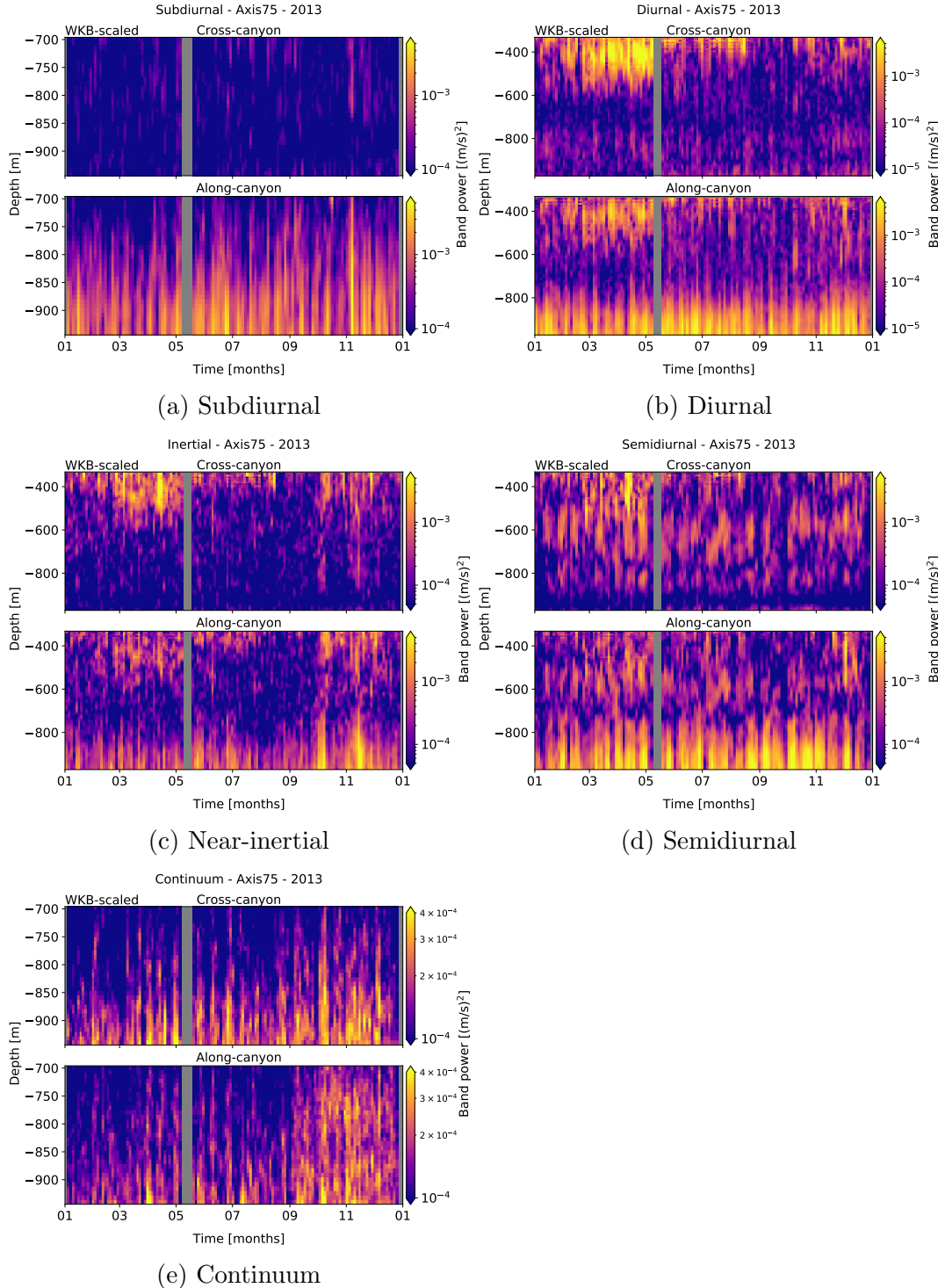


Figure 15: Band-integrated PSD data for Axis in 2013, for rotated, cleaned, and WKB-scaled horizontal velocity data. For each sub-figure, there are cross- (top) and along-slope (bottom) components. Intensity scales are adjusted for visual clarity of effects.

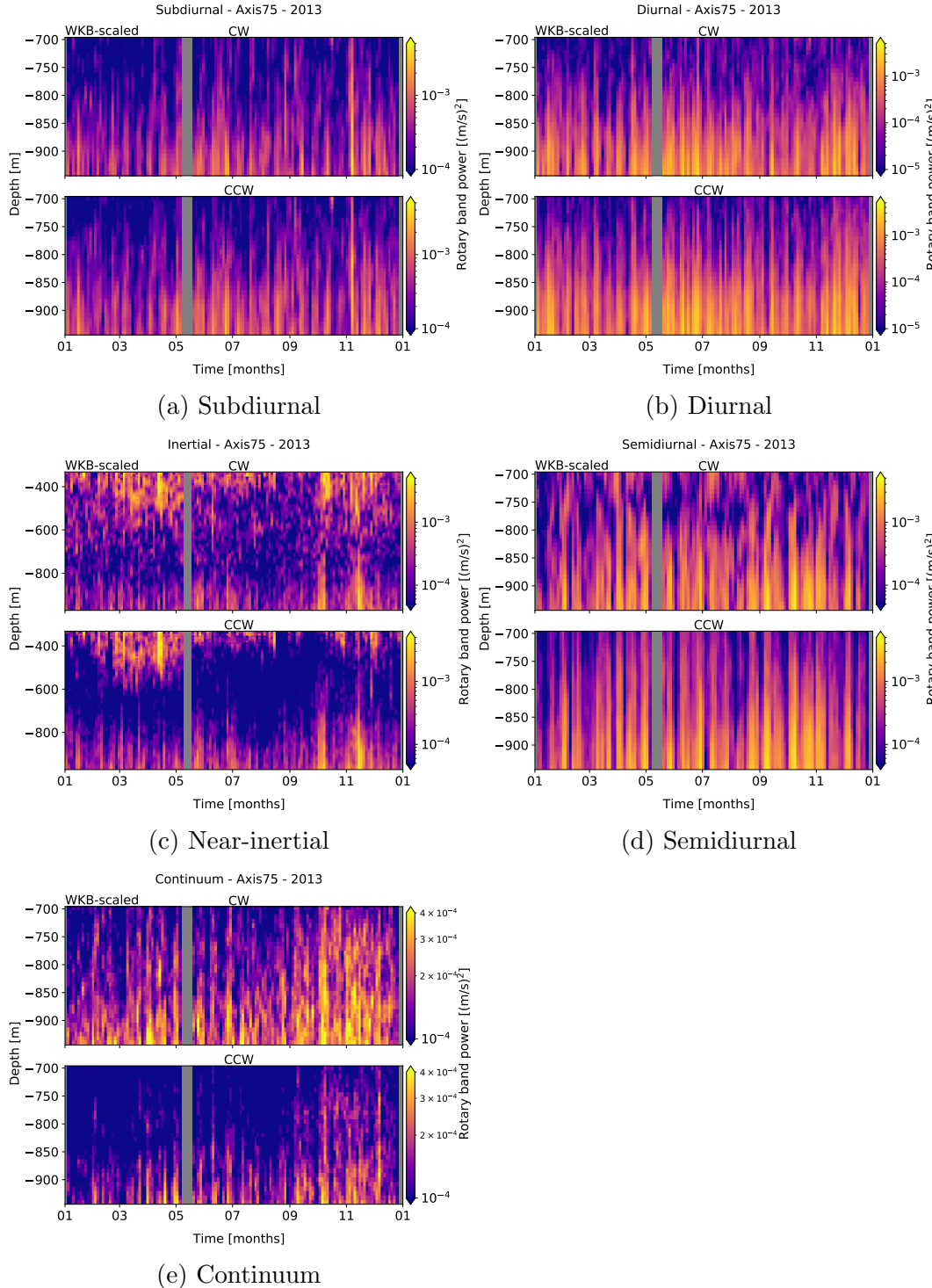


Figure 16: Band-integrated rotary data for Axis in 2013, for rotated, cleaned, and WKB-scaled horizontal velocity data. For each sub-figure, there are CW (top) and CCW (bottom) components. Intensity scales are adjusted for visual clarity of effects.

11 References